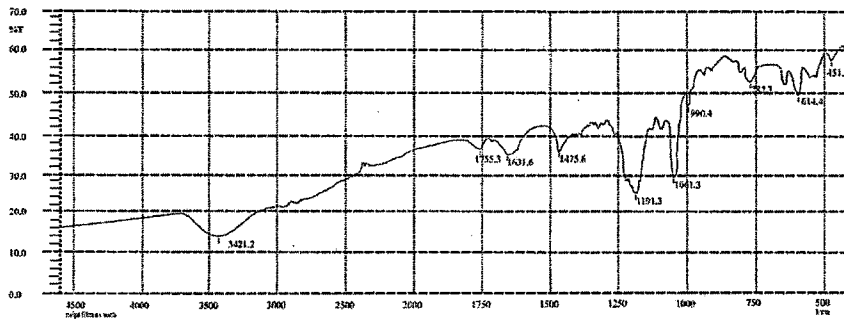


Chapter 5

Characterizations of Nanoconstructs



5.1. Introduction

Colloidal systems like nanoparticles and liposomes differ from macroscopic objects because of sub-micron properties such as high surface area and energy, and movement of the particles by diffusion (Brownian motion). The different behavior of nanoparticles and liposomes leads, to some extent, to the use of a different pattern of characterization methods. Extensive characterization of a nanoparticles system is essential for understanding and prediction of the performance of the system in the body. As the field of pharmaceutical nanoconstructs is evolving constantly; the need for more thorough characterization and comprehensive understanding of the systems increases.

Size, morphology and physical state of the encapsulated drug as well as MW and crystallinity of the polymer influence drug release and degradation of the nanoparticles.

Meanwhile, size, surface charge and hydrophobicity/hydrophilicity are parameters that affect the body distribution and interactions with the biological environment. Stability of nanoconstructs are also a general issue governing the above mentioned properties.

Various techniques for characterization of nanoparticles include:

- Photon correlation spectroscopy (PCS), a technique based on dynamic (laser) light scattering, is widely used in size determinations of nanoconstructs.
- The surface charge of the particle was determined by Zeta(ζ) Potential measurement
- The determination of drug entrapment efficiency by techniques of spectrophotometry and chromatography gives the amount of drug present in the nanoconstructs.
- The surface morphology by scanning electron microscopy (SEM), transmission electron microscopy (TEM).
- Differential scanning calorimetry (DSC) and (powder) x-ray diffractometry (XRPD) are commonly used techniques to reveal the physicochemical state and possible interactions of the drug and the polymer in nanoparticles
- The surface chemistry by Fourier transform infrared spectroscopy (FTIR), and nuclear magnetic resonance spectroscopy (NMR).
- The surface hydrophilicity of the nanoparticles influences the cellular uptake and also the *in vivo* pharmacokinetic behavior of the nanoparticles. (Sahoo, et. al., 2002) The PVA is estimated using the colorimetric iodine reaction estimated spectrophotometrically. (Joshi, D.P. et al., 1979)

Table: 5.1. Materials and Equipments

Material	Source
Water (distilled)	Prepared in laboratory by distillation
Bichinonic acid (BCA) protein Assay Kit	Banglore Genei, India
Glacial acetic acid, potassium dihydrogen phosphate, disodium hydrogen phosphate, potassium chloride, potassium hydroxide, sodium chloride, sodium hydroxide.	S.D.Fine chemicals, Mumbai, India
HPLC grade methanol, glacial acetic acid, acetonitrile	S.D.Fine chemicals, Mumbai, India
Nuclepore Polycarbonate membrane 2 μ m 25mm	Whatman, USA
Polyvinyl alcohol	Sigma Chemicals, USA
Equipments	Make
Calibrated pipettes of 1.0 ml, 5.0 ml and 10.0 ml, volumetric flasks of 10 ml, 25 ml, 50 ml and 100 ml capacity, Funnels (i.d. 5.0 cm), beakers (250 ml) and other requisite glasswares	Schott & Corning (India) Ltd., Mumbai
Analytical balance	AX 120, EL 8300, Shimadzu Corp., Japan
pH meter	Pico ⁺ Labindia, Mumbai, India
Cyclomixer, three blade stirrer	Remi Scientific Equipments, Mumbai
Cooling Centrifuge	3K 30, Sigma Laboratory centrifuge, Osterode, GmbH.
Lyophilizer	DW1, 0-60E, Heto Drywinner, Denmark
UV-Visible Spectrophotometer	Shimadzu UV-1601, Japan
Spectrofluorimeter	RF-540, Shimadzu corporation, Japan
Particle size and zeta potential analyzer	NanoZS, Malvern Instruments, U.K.
Transmission electron microscope	Morgagni, Philips, Netherlands
Differential Scanning Calorimeter	Mettler DSC 20, Mettler Toledo, Switzerland
HPLC system	Dionex HPLC with Chromleon 6.5 data processing software

5.2. Methods

5.2.1. Particle size and zeta potential: A 2.0 mg sample of nanoconstructs was suspended in distilled water, and the particle size and zeta potential were measured using the principle of laser light scattering with zeta sizer (Nano-ZS, Malvern Instruments, UK). The observations are tabulated in Table: 5.2 and Figures: 5.1 to Figure: 5.4.

5.2.2. Entrapment efficiency: To determine the amount of Docetaxel entrapped in the NPs, 2mg of NPs were added to 5 ml of methylene chloride and subjected to shaking at room temperature for 5 hrs to ensure complete dissolution of the particles. The resulting solution was evaporated to dryness, and the dried residue was reconstituted with 1 ml of mobile phase. The reconstituted solution was centrifuged and the supernatant was injected into the HPLC column. The % entrapment efficiency (EE) was calculated using the following expression.

$$\% \text{ EE} = (\text{Amount of drug in the NPs}/\text{drug added in the formulation}) * 100$$

The same process was repeated with liposomes with 5 ml of chloroform.

The results are recorded in Table: 5.2 & Table: 5.3 for nanoparticles and liposomes respectively

5.2.3. In-vitro drug release

The *in vitro* drug releases of the nanoconstructs of docetaxel were performed in phosphate buffer saline pH 7.4 + 0.1%w/v polysorbate-80 (Puglisi G., et al., 2006). Nanoconstructs equivalent to 1mg drug were suspended in 10 ml of release media in a screw capped tubes, which were placed in a horizontal shaker bath maintained at 37°C and shaken at 60min⁻¹. At fixed time intervals the tubes were taken out from the bath and centrifuged at 25,000 rpm for 30 min. The pellets were resuspended in 10ml of fresh PBS 7.4 + 0.1%w/v polysorbate-80 and placed back into the bath to continue release measurement (Feng et al., 2003b). For *in vitro* drug release study in serum the same process was repeated as above with the change of release media as 10ml of fetal bovine serum.

Results for In vitro release profile of DC encapsulated plain, and peptide tagged pegylated liposomes are tabulated in Table: 5.4 and Figure: 5.5. Results for In vitro release profile of DC encapsulated plain, and peptide tagged nanoparticles are tabulated in Table: 5.5

and Figure: 5.6. Results of in vitro serum study for nanoconstructs are shown in Figure:

5.7.

5.2.3. Transmission electron microscopy

Nanoconstructs were dispersed in de-ionized water at a concentration of 500 μ g/ml. To measure the morphology and size distribution of nanoparticles, a drop of sample was placed onto a 300-mesh copper grid coated with carbon. The grid was air-dried overnight to remove surface water. The images were taken for Nanoparticles without negative staining. While in case of liposomes, negative staining was performed using a droplet of 0.5% w/v phosphotungstic acid. Transmission electron microscopy was performed using Morgagni 268, Philips (Netherlands) transmission electron microscope. The TEM RGD conjugated nanoparticles and liposomes for docetaxel are shown in Figure: 5.8 and Figure: 5.9, respectively.

5.2.4. Surface morphology

The morphology was examined by scanning electron microscopy (SEM) (JSM-5610LV, JEOL, Japan). Samples were attached to sample stubs using double sided tape, and then viewed using an accelerating voltage of 15 kilovolt at the magnification of 250X to 20000X. Results are recorded in Figure: 5.10 and Figure: 5.11 for DC encapsulated nanoparticles and liposomes, respectively.

5.2.5 X- ray diffraction studies (XRD)

Powder X-ray diffraction patterns were obtained using an X-ray diffractometer (Philips PW 1710) with Cu K α radiation generated at 30 mA and 40 kV. The source of X - ray was copper anode with a wavelength of 1.54060 Å. The XRD patterns were recorded for DC, PLGA, PLGA-DC NPs, PLGA-DC-RGD NPs, HSPC-SPC-DC LPs and HSPC-SPC-DC-RGD LPs. Results are recorded in Figure: 5.12 and Figure: 5.13 for nanoparticles and liposomes, respectively.

5.2.6. Differential Scanning Colorimetry:

The DSC of DC, PLGA, PLGA-DC NPs, PLGA-DC-RGD NPs, HSPC-SPC-DC LPs and HSPC-SPC-DC-RGD LPs was carried out by scanning the samples using differential scanning calorimeter (Mettler). Thermograms were analyzed using Mettler Toledo star SW 7.01. An empty aluminium pan was used as the reference for all measurements. During each scan, 2 to 3 mg of sample was heated, in a hermetically sealed aluminium pan, at a heating rate of 10° C/min, from 25° C to 300° C, under a nitrogen atmosphere.

Figures: 5.14 and Figure: 5.15 show the differential scanning calorimetric grams for nanoparticles and liposomes, respectively.

5.2.7. Determination of residual PVA

The amount of PVA associated with nanoparticles was determined by a colorimetric method based on the formation of a colored complex between two adjacent hydroxyl groups of PVA and an iodine molecule (Joshi, D.P. et al., 1979). Briefly, 2 mg of lyophilized nanoparticles sample was treated with 2 ml of 0.5 M NaOH for 15 min at 60 °C. Each sample was neutralized with 900 ml of 1 N HCl and the volume was adjusted to 5 ml with distilled water. To each sample, 3 ml of a 0.65 M solution of boric acid, 0.5 ml of a solution of I₂/KI (0.05 M/0.15 M), and 1.5 ml of distilled water were added. Finally, the absorbance of the samples was measured at 690 nm after 15 min incubation. A standard plot of PVA was prepared under identical conditions.

5.2.8. ¹H-NMR of the RGD conjugated nanoconstructs

¹H-NMR spectroscopy was used to ascertain the conjugation of RGD to the nanoconstructs. The ¹H-NMR spectra of PLGA, PLGA-DC-RGD NPs, LPs and RGD-DC-LPs are shown in Figure: 5.16 a, b, c and d, respectively.

5.2.9 Infrared spectra of nanoparticles

Infrared spectra of the drug loaded unconjugated and the RGD conjugated nanoparticles and liposomes were obtained (Figure: 5.17a, b, c and d) and analyzed for confirmation of the RGD conjugation.

5.3. Results and Discussion:

5.3.1. Particle size, zeta potential and drug entrapment efficiency

The particle size, zeta potential and drug entrapment efficiency (%EE) for PLGA-DC-NP and PLGA-DC-RGD-NP are recorded in Table: 5.2. The particle size and zeta potential are shown in Figure: 5.1 and Figure: 5.2, respectively.

Table: 5.2. Characterization of optimized RGD conjugated and unconjugated PLGA nanoparticles of Docetaxel

Parameter	* PLGA-DC-NP	# PLGA-DC-PEG-NP	** PLGA-DC-PEG-RGD-NP
Mean particle size (nm)	210.3 ± 2.7	221.4 ± 1.6	230.7 ± 2.3
Zeta potential (mV)	-38.4 ± 2.6	-11.3±1.8	-10.2 ± 2.8
Entrapment efficiency (%)	71.6 ± 2.4 %	59.7 ± 3.3	58.4 ± 1.6

(Mean ± S.D., n = 3)

* PLGA-DC-NP- Docetaxel loaded PLGA nanoparticles

PLGA-DC-PEG-NP –pegylated Docetaxel loaded PLGA nanoparticles

** PLGA-DC-PEG-RGD-NP- RGD conjugated docetaxel loaded PLGA nanoparticles

Figure: 5.1. Particle size distribution plots of docetaxel loaded PLGA nanoparticles, before and after RGD conjugation.

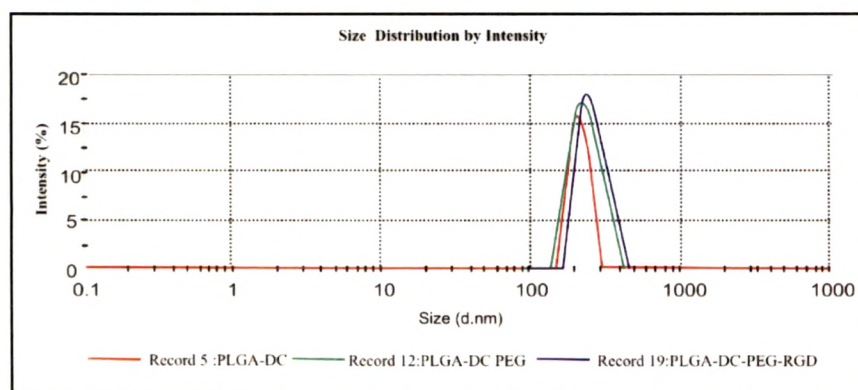


Figure: 5.2. Zeta Potential plots of docetaxel loaded PLGA nanoparticles, before and after RGD conjugation.

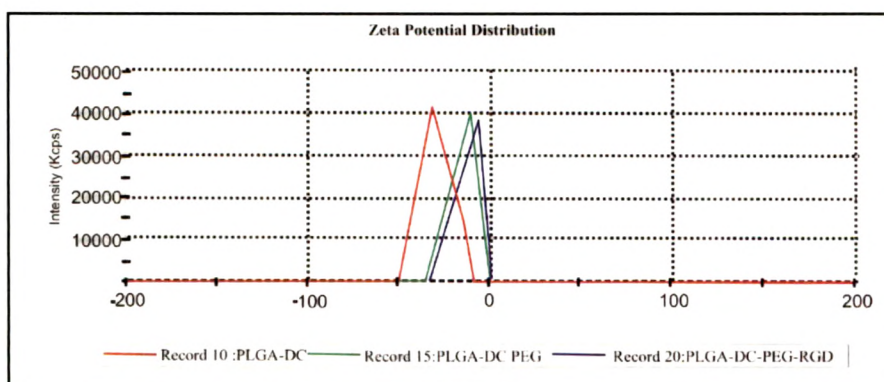


Figure: 5.3. Particle size distribution plots of docetaxel loaded Liposomes, before and after RGD conjugation.

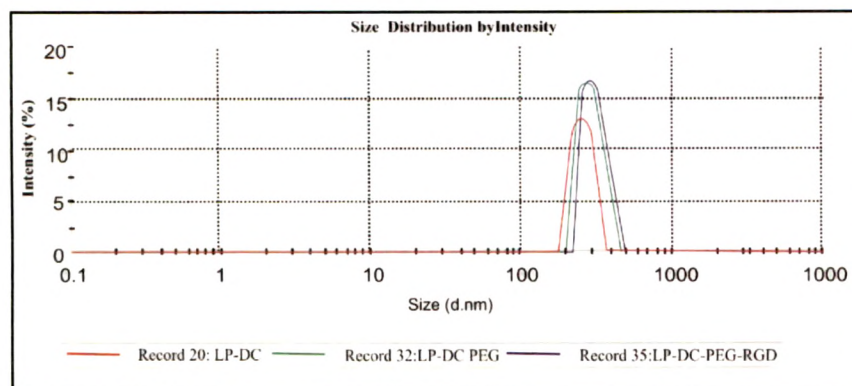


Figure: 5.4. Zeta Potential plots of docetaxel loaded liposomes before and after RGD conjugation.

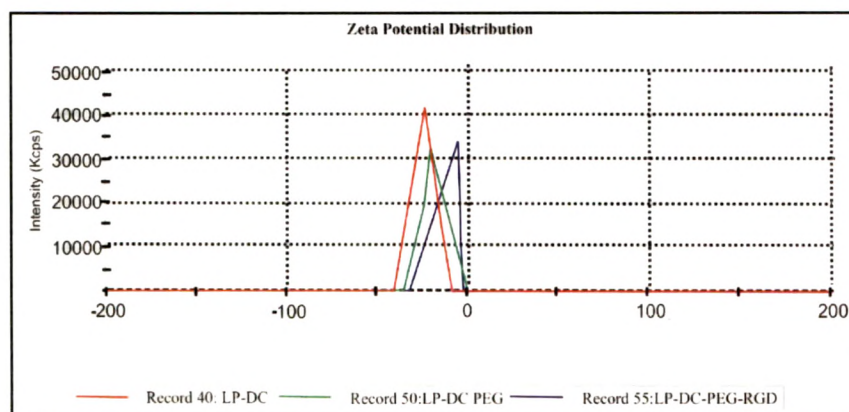


Table: 5.3.Characterization of optimized RGD conjugated and unconjugated Liposomes of Docetaxel

Parameter	* LP-DC	# LP-DC-PEG	**LP-DC-PEG-RGD
Mean particle size (nm)	260.4 ± 4.6	269.2 ± 2.8	278.6±3.4
Zeta potential (mV)	-28.7 ± 1.3	-27.2±1.8	-11.6±0.4
Entrapment efficiency (%)	72.8 ± 2.2 %	69.2±5.8	64.5±1.5

(Mean ± S.D., $n = 3$)

* LP-DC Docetaxel loaded Liposomes

LP-DC-PEG Docetaxel loaded pegylated liposomes

**LP-DC-PEG-RGD – RGD conjugated Docetaxel loaded Liposomes

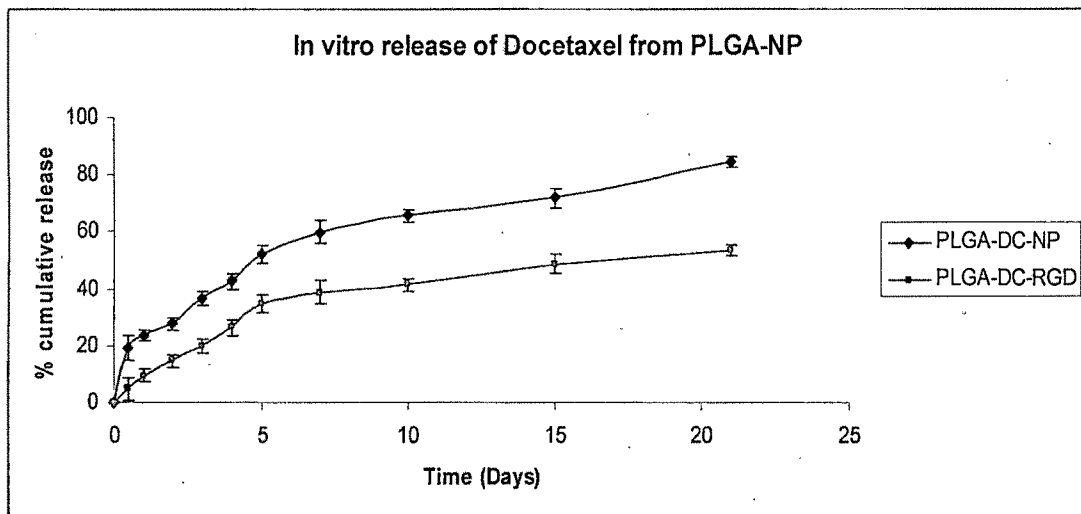
Mean particle size and zeta potential of PLGA-DC-NP and PLGA-DC-RGD-NP were found to be $210.3 \pm 2.7\text{nm}$ and $-38.4 \pm 2.6\text{mV}$ and $230.7 \pm 2.3\text{nm}$ and $-10.2 \pm 2.8\text{mV}$ respectively. Increase in the particle size after RGD conjugation was due to RGD conjugated. The %EE for PLGA-DC-NP and PLGA-DC-RGD-NP was found to be $71.6 \pm 2.4\%$ and $58.4 \pm 1.6\%$ respectively. The reduced drug entrapment efficiency for PLGA-DC-RGD-NP may be due to dissociation of the drug on the surface of PLGA-DC-NP during the RGD conjugation process.

Similarly, the particle size and zeta potential for LP-DC, LP-DC-PEG and LP-DC-RGD are recorded in Table: 5.3. The particle size and zeta potential are shown in Figure: 5.3 and Figure: 5.4, respectively. Mean particle size and zeta potential of LP-DC & LP-DC-PEG were found to be $260.4 \pm 4.6\text{nm}$ & $269.2 \pm 2.8\text{nm}$ and -28.7 ± 1.3 & $-27.2 \pm 1.8\text{mV}$ respectively. While the LP-DC-PEG-RGD demonstrated $278.6 \pm 3.4\text{nm}$ particle size and $-11.6 \pm 0.4\text{mV}$ zeta potential. The %EE for LP-DC, LP-DC-PEG and LP-DC-PEG-RGD was determined to be $72.8 \pm 2.2\%$, $67.9 \pm 3.1\%$ and $64.5 \pm 1.5\%$, respectively.

5.3.2. In-vitro Drug Release

Release of the entrapped therapeutic agent from PLGA matrix has been found to occur through diffusion-cum-degradation-mediated processes (Crotts, G. et al., 1998). It has been demonstrated that during the early phases, the release of the entrapped therapeutic agent occurs mainly through its diffusion in the polymer matrix while during the later phases, the release is mediated through both diffusion of the therapeutic agent and the degradation of the polymer matrix itself. Thus, degradation rate of the polymer matrix is an important determinant of the in vitro release of the therapeutic agent from PLGA matrices (Anderson, J.M. et al., 1997). The acidic (lactic acid and glycolic acid) monomers and oligomers formed catalyze the further degradation of the parent polymer. Thus, any factor that influences the formation and/or retention of the acidic monomers in the particles could affect the polymer degradation rate and the in vitro release of the entrapped therapeutic agent (Panyam, J. et al., 2003).

Figure: 5.5. In-vitro release of Docetaxel from PLGA NPs before and after conjugation with RGD



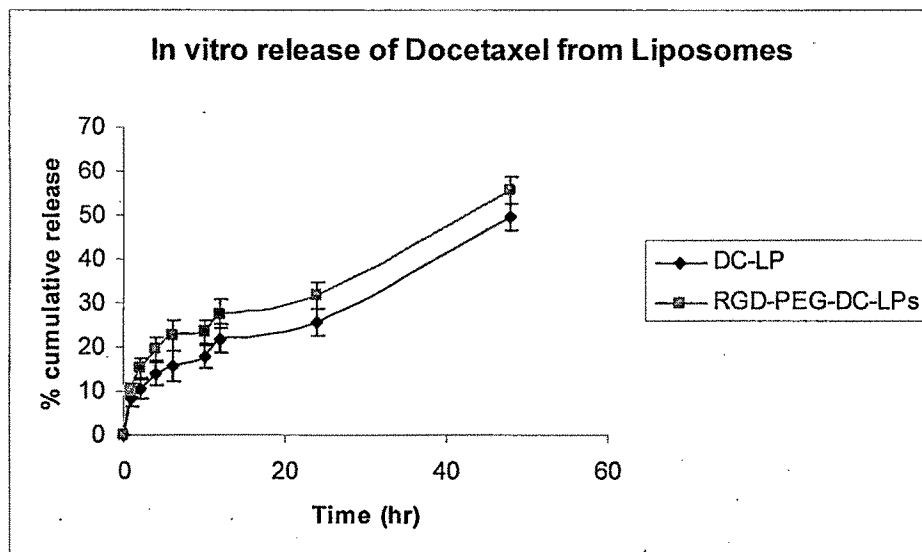
(Mean \pm S.D., $n = 3$)

* PLGA-DC-NP- Docetaxel loaded PLGA nanoparticles

PLGA-DC-RGD-NP – RGD conjugated Docetaxel loaded PLGA nanoparticles

The release studies of Docetaxel from the optimized nanoparticle batch were conducted in phosphate buffer pH 7.4 + 0.1%w/v polysorbate-80. The release curves of PLGA-DC-NP and PLGA-DC-RGD-NP are shown in Figure: 5.5. For PLGA-DC-NP there was an initial burst release of about 19% in 12hrs and then there was a lag phase and about 80% release resulted in 21 days. The unconjugated nanoparticles showed a high initial burst which can be attributed to the immediate dissociation and dissolution of drug adhered on the surface and located near the surface of the NPs (Magenheim, et al., 1993). While in lag phase, the release is mainly due to the erosion of the polymer matrix and further diffusion of drug molecules through the polymeric matrix of the NPs. The matrix material would require time to erode in the aqueous environment than the release mechanisms of surface release, resulting in the prolonged release. (Esmaeili, F. et al., 2008). The burst effect was absent in PLGA-DC-RGD-NP and the release in 21 days was found to be about 60%. The release studies of Docetaxel from the optimized liposomes batch were conducted in phosphate buffer pH 7.4 + 0.1%w/v polysorbate-80.

Figure: 5.6. In-vitro release of Docetaxel from Liposomes before and after conjugation with RGD



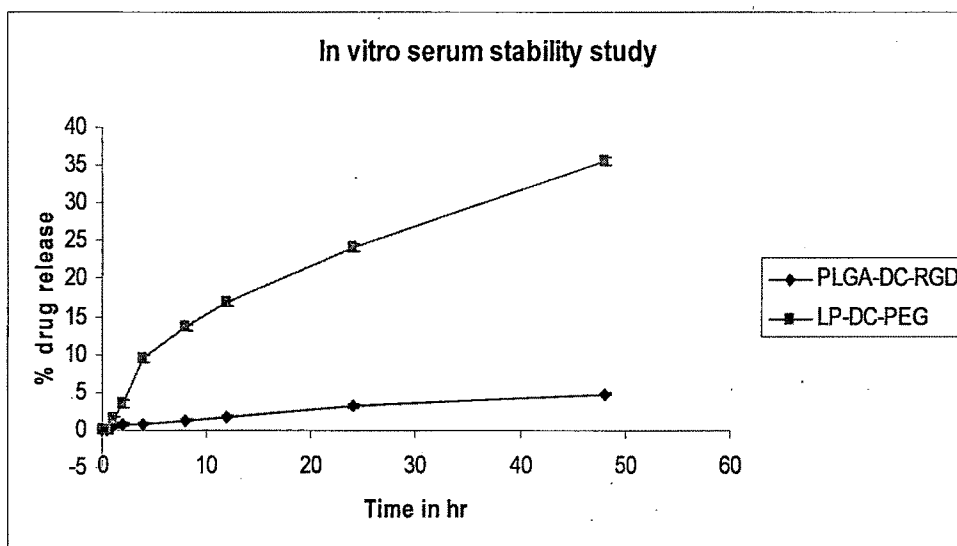
(Mean \pm S.D., $n = 3$)

* LP-DC Docetaxel loaded Liposomes

LP-DC-PEG-RGD – RGD conjugated Pegylated Docetaxel loaded Liposomes

In vitro drug release from Docetaxel-loaded, non-pegylated and RGD conjugated pegylated liposomes is summarized in the cumulative percentage release shown in Figure: 5.6. It was found that both formulations produced an initial burst release in which docetaxel release was more than 10 % and 8 % for pegylated and non-pegylated liposomes, respectively, within the initial sampling time (30min). The burst release in both forms of liposomes is related to release of surface adsorbed drug. After the initial burst release, a constant drug release was found and maximum of 75% and 60% drug was released in 48hr of time period with pegylated and non pegylated liposomes respectively. Faster release in pegylated liposomes may be due to the fast hydration process of PEG molecules on the surface of the particles.

Figure: 5.7. In vitro serum drug release for RGD-PEG-DC-NPs and RGD-PEG-DC-LPs



In vitro drug release from DC encapsulated RGD conjugated pegylated liposomes and from DC encapsulated RGD conjugated pegylated nanoparticles was about 35.6% and 4.8% respectively in 48 hrs. The difference of drug release may be attributed to the hydrophobic nature of PLGA.

5.3.3. Transmission Electron Microscopy

The TEM RGD conjugated nanoparticles and liposomes for Docetaxel are shown in Figure: 5.8 and Figure: 5.9, respectively. TEM images NPs & LPs showed spherical NPs & LPs with smooth surfaces.

Figure: 5.8. Morphology of Docetaxel nanoparticles using TEM

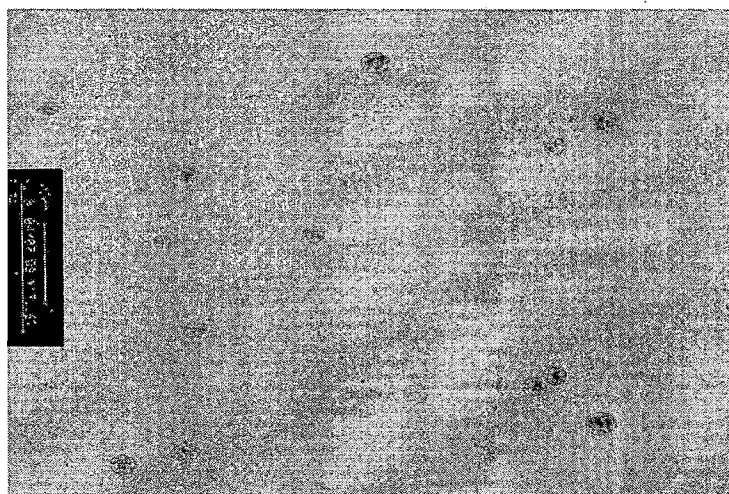
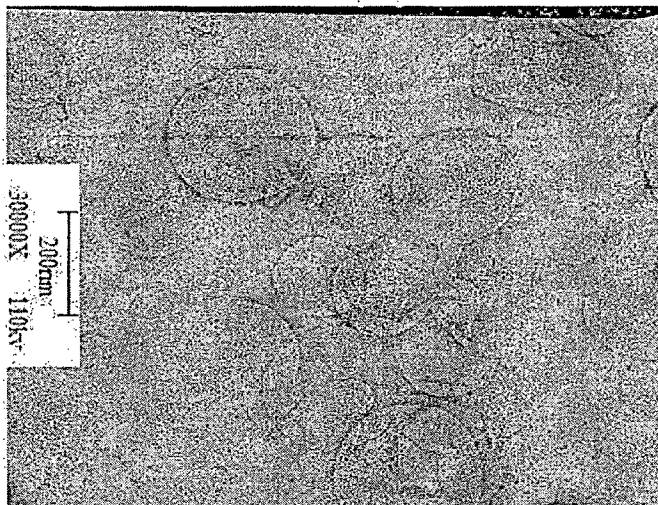


Figure: 5.9. Morphology of Docetaxel liposomes using TEM



5.3.4. Scanning Electron Microscopy

The SEM images for DC nanoparticles and Liposomes are shown in Figure 5.10 and Figure 5.11, respectively. SEM images of nanoconstructs showed spherical shape with smooth surfaces and the sphericity did not alter significantly after conjugation.

Figure: 5.10. Morphology of Docetaxel nanoparticles using SEM

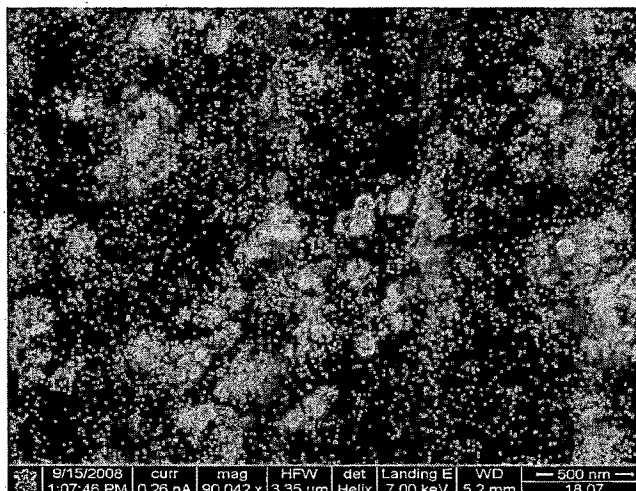
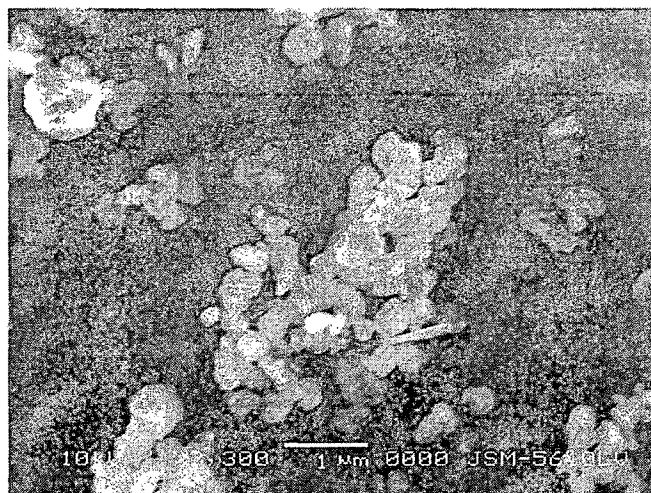


Figure: 5.11. Morphology of Docetaxel liposomes using SEM

5.2.5. X- ray diffraction studies (XRD)

Crystal diffraction software tools are widely used to simulate XRD patterns as reference standards for individual crystal forms (such as polymorph, solvates, and salts). The XRD pattern of bulk DC showed a total of 12 peaks while the XRD patterns of RGD-DC-PLGA NPs and RGD-DC-LPs did not showed any characteristic peaks. The crystallinity index of DC after conversion into nanoparticles was calculated by considering the intensity of the principle peak obtained with bulk DC as 100%. Results are recorded in Figure: 5.12 and Figure 5.13 for nanoparticles and liposomes, respectively.

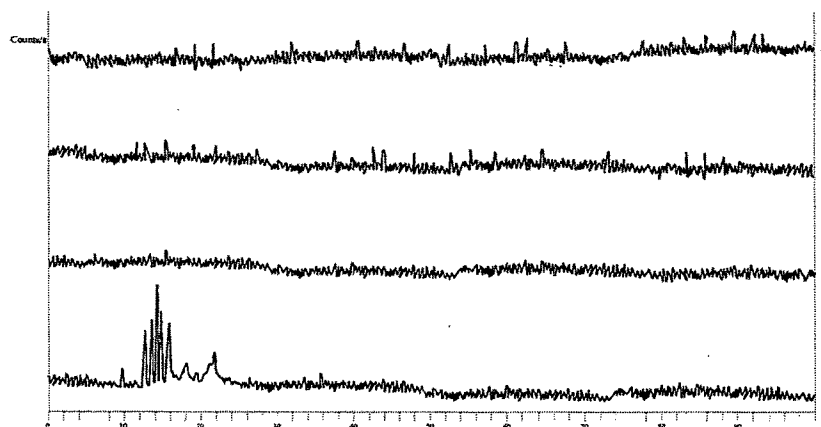
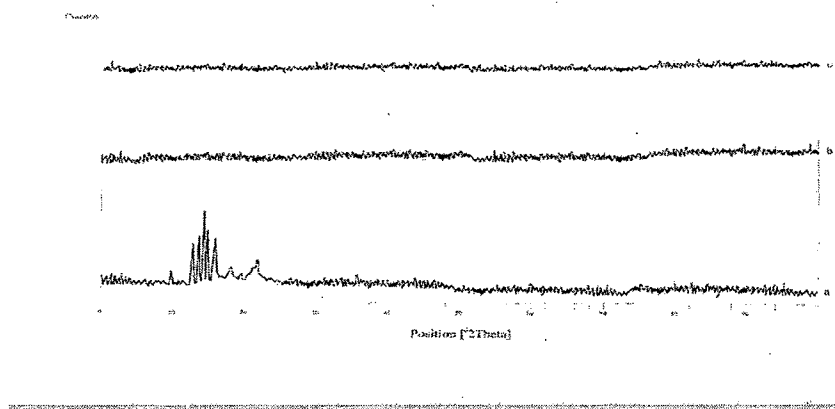
Figure: 5.12. XRD photograph of (a) free drug,(b) non PEGylated PLGA NPs, (c) PEG-DC-PLGA NPs and d) RGD-PEG-DC-PLGA NPs

Figure: 5.13. XRD photograph of (a) free drug,(b) non PEGylated liposomes, (c) RGD-PEG-DC liposomes



5.3.6. Differential Scanning Calorimetry

The physical state of the drug in nanoparticles can be determined by differential scanning calorimetry (DSC). The drug can exist in different polymorphic forms in the formulations i.e. amorphous or crystalline.

DSC thermogram of plain Docetaxel shown in Figure: 5.15 depicts a sharp melting peak from 169-171°C, indicating the crystalline nature of the drug. The drug in the amorphous form is entrapped in the nanoparticles. For PLGA-DC-NP, as shown in Figure: 5.15, the peak of Docetaxel is absent indicating the conversion of DC into amorphous state during the nanoparticles formulation and thereby entrapped in the PLGA polymer.

Similarly, for LP-DC as in Figure: 5.14, the peak of docetaxel is absent indicating the conversion of DC into amorphous state during the liposome formulation and thereby entrapped in the liposomes.

Figure: 5.14. DSC analysis (b) free drug,(a) PEGylated liposomes, (c) physical mixture of HSPC,SPC,cholesterol,DSPE-PEG2000, (d)HSPC

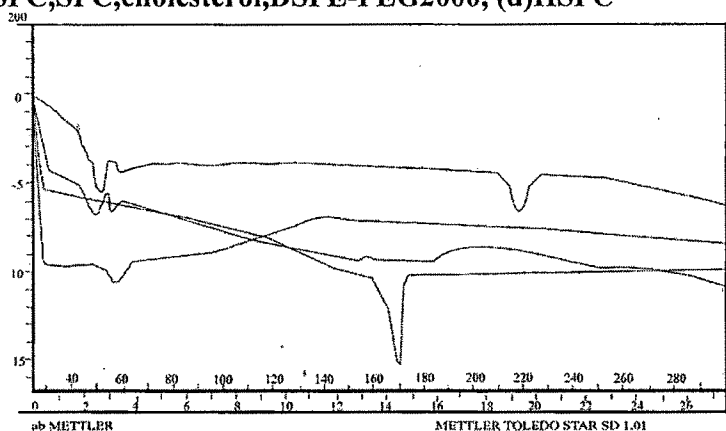
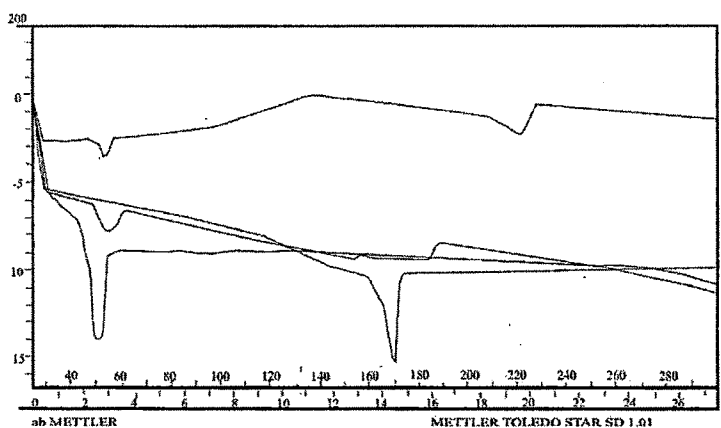


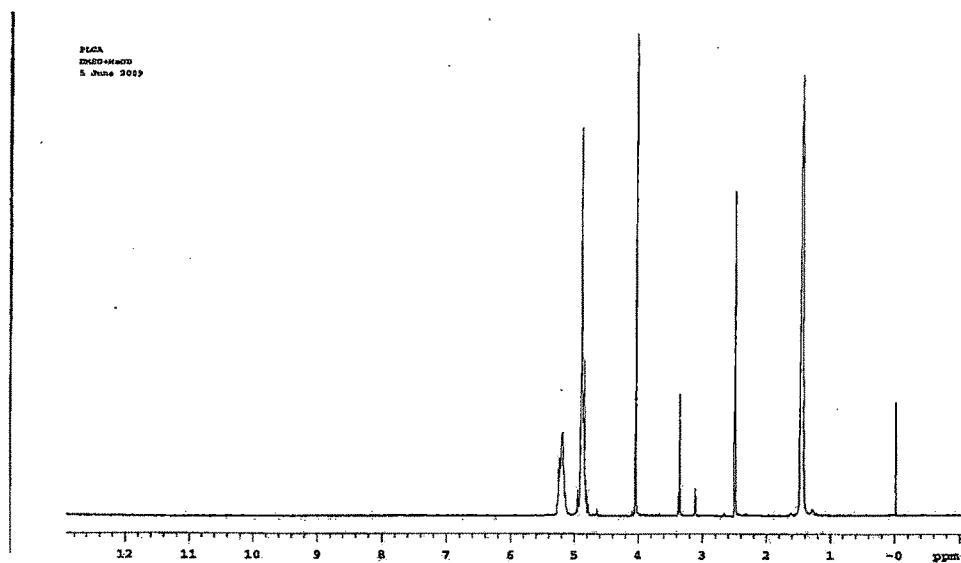
Figure: 5.15 DSC analysis (b) free drug,(a) PEGylated nanoparticles, (c) PLGA (d)RGD-PEG-DC-PLGA NPs



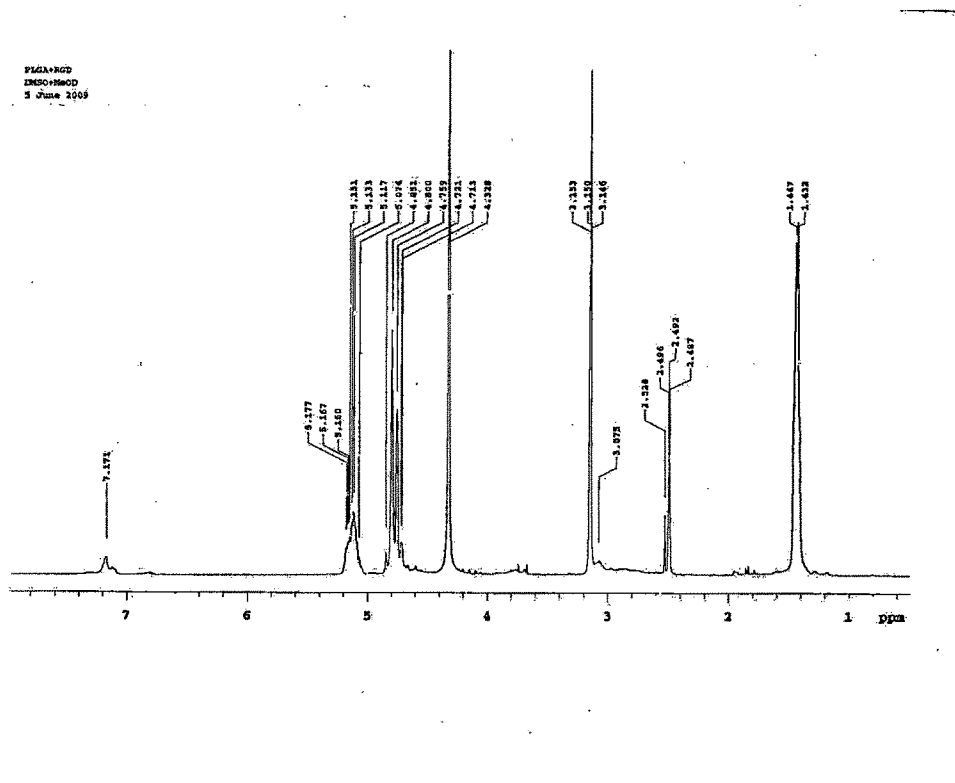
5.3.7. ^1H NMR of the RGD conjugated nanoconstructs

^1H -NMR spectroscopy was used to ascertain the conjugation of RGD to the nanoconstructs. The ^1H -NMR spectra of PLGA, PLGA-DC-RGD NPs, LPs and RGD-DC-LPs are shown in Figure:5.16 a, b, c and d, respectively.

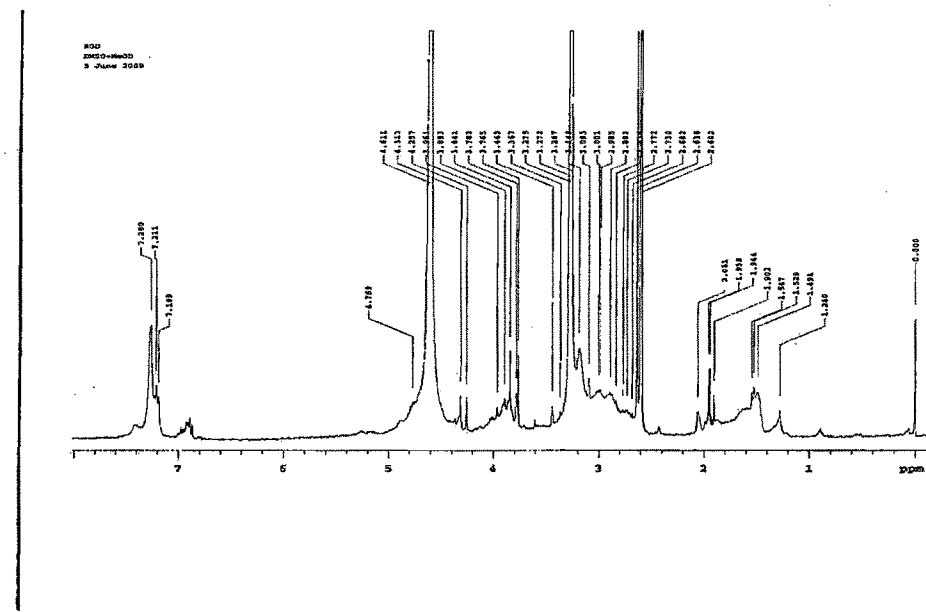
Figure: 5.16. ¹H-NMR spectra of (a) PLGA, (b) PLGA-DC-RGD NPs, (c)RGD and (d) RGD-DC-LPs



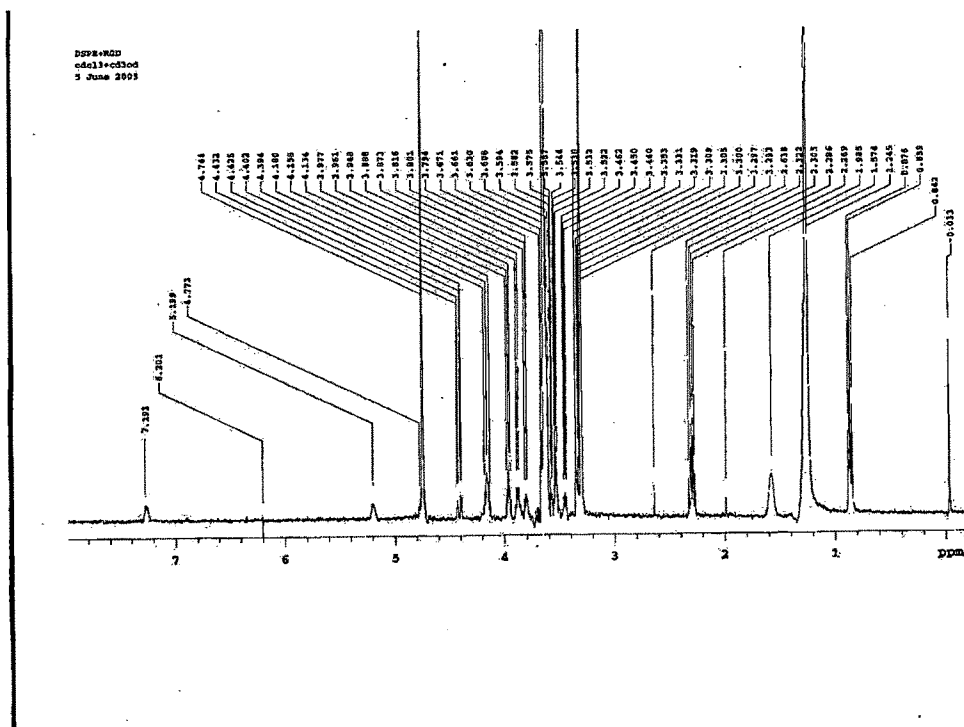
(a)



(b)



(c)



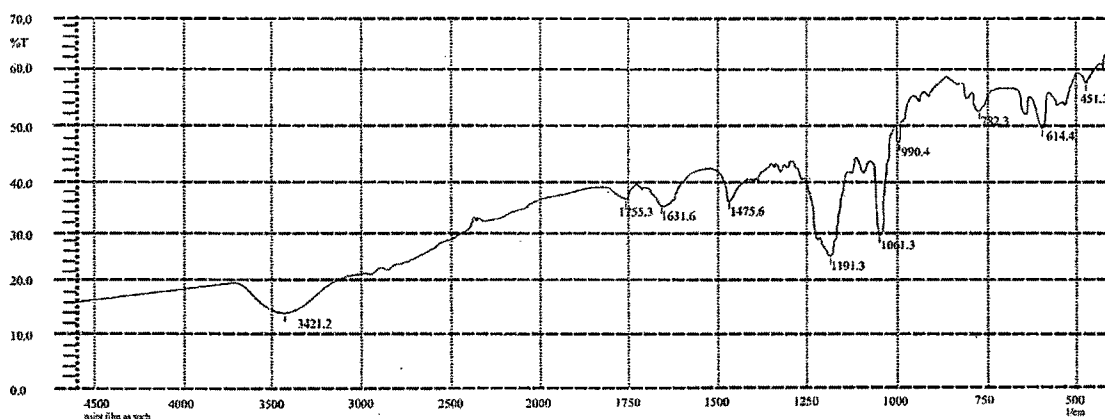
(d)

The presence of characteristic peak at δ value 7.1 reveals the presence of RGD with nanoparticles (Figure 5.16b) and liposomes (Figure 5.16d). The unconjugated PLGA nanoparticles did not show any peak at 7.1, which depicts the absence of RGD.

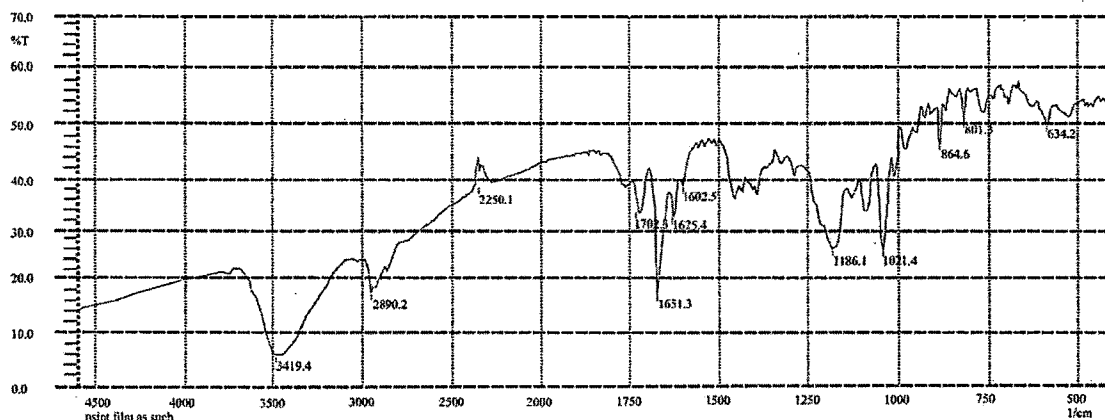
5.3.8. Infrared spectra of nanoparticles

Infrared spectra of the drug loaded unconjugated and the RGD conjugated nanoparticles and liposomes were obtained (Figure: 5.17 a, b, c and d) and analyzed for confirmation of the RGD conjugation.

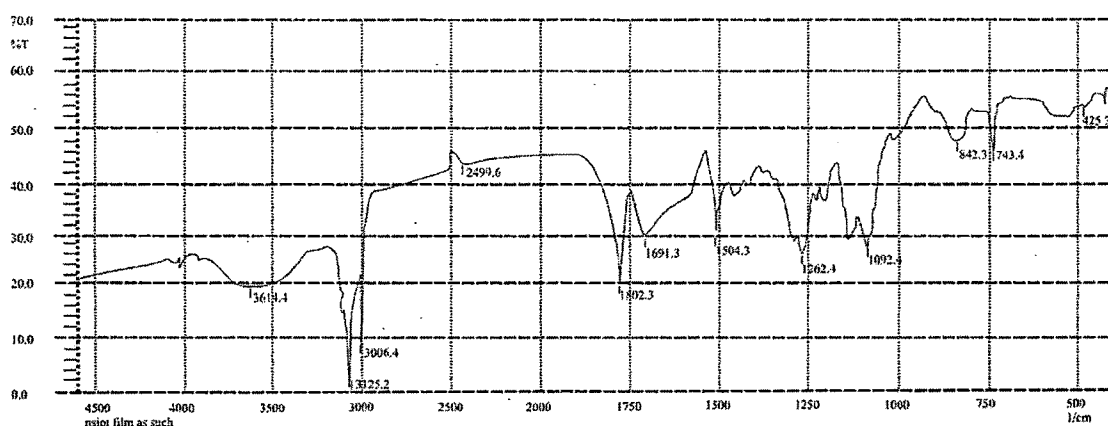
Figure: 5.17. FTIR spectra of (a) DC-PLGA NPs, (b) RGD-DC-PLGA NPs, (c) DC-PEG-LPs and (d) RGD-DC-PEG-LPs



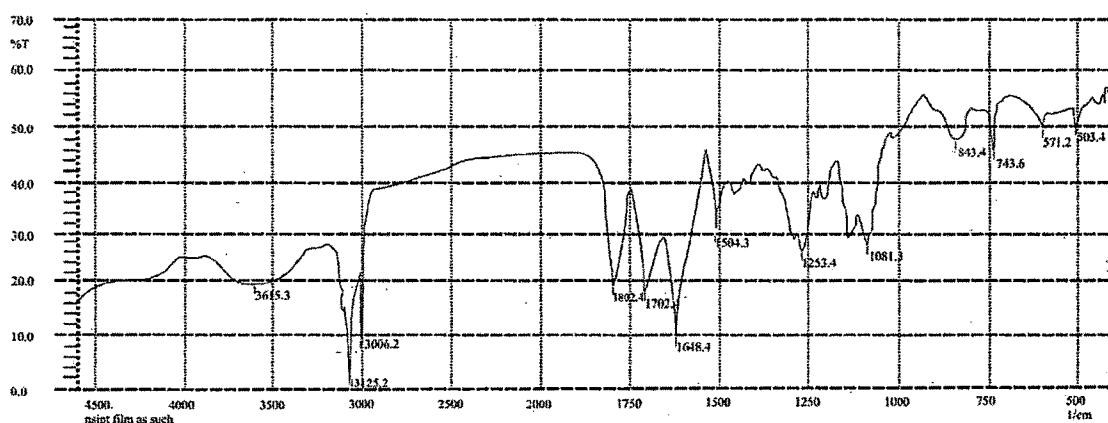
(a)



(b)



(c)



(d)

The peaks at 1625 cm^{-1} , 1651 cm^{-1} and 1648 cm^{-1} in the IR spectra of RGD-DC-NPs and RGD-DC-LPs respectively indicated the presence of amide (CO-NH) group. This confirms the conjugation of RGD onto the surface of nanoconstructs. While the aforesaid peaks are absent in unconjugated nanoconstructs.

5.3.9. Residual PVA

The residual PVA associated with the nanoparticles surface was $7.4 \pm 2.1\%$ and $5.4 \pm 1.3\%$ w/w of unconjugated and conjugated docetaxel encapsulated nanoparticles respectively.

5.3.10. Characterization of 6-coumarin nanoparticles

Unconjugated and RGD conjugated fluorescent NPs and liposomes encapsulating 6-coumarin required for studying cellular uptake of NPs by breast cancer cells were

prepared and characterized by the same methods used for drug loaded NPs & LPs and the results are recorded in Table:5.4. and Table: 5.5, respectively.

Table: 5.4. Characterization of 6- coumarin nanoparticles

Character	6-coumarin nanoparticles	
	Unconjugated	RGD conjugated
Particle size (nm)	247.4 ± 4.5	321.3 ± 8.4
Zeta potential (mV)	-12.6 ± 1.4	-10.3 ± 1.5
Entrapment Efficiency	92.21 ± 3.61	84.47 ± 3.41
Surface RGD (µg /mg)	----	32.3 ± 2.6
Residual PVA (% w/w)	7.4 ± 2.1	5.4 ± 1.3

Table: 5.5. Characterization of 6- coumarin liposomes

Character	6-coumarin nanoparticles	
	Unconjugated	RGD conjugated
Particle size (nm)	267.5 ± 5.2	293.6 ± 7.3
Zeta potential (mV)	-27.4 ± 2.5	-11.5 ± 3.4
Entrapment Efficiency	90.16 ± 4.22	82.53 ± 4.62
Surface RGD (µg /mg)	----	36.4 ± 3.5

6-coumarin loaded unconjugated NPs and RGD-conjugated NPs had a particle size of 247.4 ± 4.5 nm and 321.3 ± 8.4nm and zeta potential of -12.6 ± 1.4 mV and -10.3 ± 1.5 mV respectively. RGD conjugated NPs had 32.3 ± 2.6 µg RGD /mg of nanoparticles. The entrapment efficiency as evaluated using spectrofluorimetry was found to be 92.21 ± 3.61 and 84.47 ± 3.41 for unconjugated and conjugated 6-coumarin nanoparticles. The residual PVA was found to be 7.4 ± 2.1 % and 5.4 ± 1.3 % for unconjugated and transferrin conjugated nanoparticles respectively. The particle size, zeta potential, the surface density of RGD and residual PVA of 6-coumarin NPs were found to be similar to the drug loaded NPs. So it is expected that their cellular uptake would be similar to that of the drug loaded NPs.

5.4. Conclusions

After characterization we can conclude that the unconjugated and RGD conjugated nanoconstructs of docetaxel have small particle size (<300nm) suitable for intravenous administration. A prolonged release was observed for both unconjugated and conjugated nanoconstructs of docetaxel. The smooth and spherical surface of nanoconstructs was confirmed from TEM and SEM. The DSC & XRD studies indicate the presence of the drug in nanoconstructs in the amorphous form.

The unconjugated and RGD conjugated nanoconstructs of Docetaxel were further subjected to stability studies according to ICH guidelines (Chapter 6).

5.5. References:

Anderson, J .M. 1997, Biodegradation and biocom- PLA and PLGA microspheres, *Adv. Drug. Deliv. Rev.*, **28**, 5–24.

Atyabi, F et al., 2009, Preparation of pegylated nano-liposomal formulation containing SN-38: *In vitro* characterization and *in vivo* biodistribution in mice, *Acta Pharm.*, **59**, 133–144.

Boury, F. et al., 1995, Dynamic properties of poly (D,L-lactide) and polyvinyl alcohol monolayers at the air/water and dichloromethane air/water interfaces. *J. Colloid. Interf. Sci.*, **169**, 380–392.

Crotts, G. et al., 1998, Protein delivery from poly(lactic- glycolic acid) biodegradable microspheres: release kinetics and stability issues, *J. Microencapsul.* **15**, 699–713.

Esmacili, F. et al., 2008, PLGA nanoparticles of different surface properties: Preparation and evaluation of their body distribution, *International Journal of Pharmaceutics*, **349**, 249–255.

Jagdish Singh et al., 2000, Effect of Isopropyl Myristic Acid Ester on the Physical Characteristics and In Vitro Release of Etoposide from PLGA Microspheres, *AAPS. Pharm.Sci.Tech.*, **1(4)**, article 32.

Joshi, D.P. et al., 1979, Determination of poly (vinyl alcohol) via its complex with boric acid and iodine, *Anal. Chim. Acta.*, **104**, 153–160.

Magenheim, B. et al., 1993, A new in vitro technique for evaluation of drug release profile from colloidal carriers-ultrafiltration technique at low pressure, *Int. J. Pharm*, **94**, 115–123.

Mu, L. et al., 2002, Vitamin E TPGS used as emulsifier in the solvent evaporation/extraction technique for fabrication of polymeric nanospheres for controlled release of paclitaxel (Taxols), *J. Control. Rel*, **80**, 129–144.

Sanjeeb, K. et al., 2002, Residual polyvinyl alcohol associated with poly (lactide-co-glycolide) nanoparticles affects their physical properties and cellular uptake, *Journal of Controlled Release*, **82(1)**, 105-114.

Shen Gao et al., 2007, Temozolomide/PLGA microparticles and antitumor activity against Glioma C6 cancer cells in vitro, *Int. J. of Pharm.*, **329 (1-2)**, 122-128.

Chapter 5	218
5.1. Introduction	219
5.2. Methods	221
5.2.1. Particle size and zeta potential.....	221
5.2.3. In-vitro drug release.....	221
5.2.3. Transmission electron microscopy	222
5.2.4. Surface morphology	222
5.2.5 X- ray diffraction studies (XRD).....	222
5.2.6. Differential Scanning Colorimetry	222
5.2.7. Determination of residual PVA	223
5.2.8. [¹ H]NMR of the RGD conjugated nanoconstructs	223
5.2.9 Infrared spectra of nanoparticles	223
5.3. Results and Discussion:	223
5.3.1. Particle size, zeta potential and drug entrapment efficiency	223
5.3.2. In-vitro Drug Release	226
5.3.3. Transmission Electron Microscopy	229
5.3.4. Scanning Electron Microscopy.....	230
5.2.5. X- ray diffraction studies (XRD).....	231
5.3.6. Differential Scanning Calorimetry	232
5.3.7. [¹ H]NMR of the RGD conjugated nanoconstructs	233
5.3.8. Infrared spectra of nanoparticles	236
5.3.9. Residual PVA	237
5.3.10. Characterization of 6-coumarin nanoparticles.....	237
5.4. Conclusions	239
5.5. References:	240